11

Koyi, H. A., M. Sans, A. Teixell, J. Cotton, and H. Zeyen, 2003, The significance of penetrative strain in the restoration of shortened layers—Insights from sand models and the Spanish Pyrenees, *in* K. R. McClay, ed., Thrust tectonics and hydrocarbon systems: AAPG Memoir 82, p. 1–16.

The Significance of Penetrative Strain in the Restoration of Shortened Layers—Insights from Sand Models and the Spanish Pyrenees

Hemin A. Koyi

Hans Ramberg Tectonic Laboratory, Department of Earth Sciences, Uppsala University, Uppsala, Sweden

Maura Sans

Departament de Geologia Dinamica, Geofisica i Paleontologia, Universitat de Barcelona, Barcelona, Spain

Antonio Teixell

Departament de Geologia (Geotectonica), Universitat Autonoma de Barcelona, Bellaterra, Spain

James Cotton[1]

Chertsey Road, Sunbury-on-Thames, Middlesex, U.K.

Hermann Zeyen

Dép. des Sciences de la Terre, Université de Paris-Sud, Orsay cedex, France

ABSTRACT

Dynamic restoration is achieved when one accounts for the changes that occur in area or volume during deformation. In contractional areas, layer-parallel shortening (LPS) cannot always be easily estimated or measured, although it is a significant component of deformation, as is gravitational compaction. Five model analogs with known initial dimensions and boundary conditions were shortened from one end. Profiles of these models were used to (1) estimate the amount of layer-parallel compaction (LPC), the main modality of layer-parallel shortening in granular analog materials; (2) outline variation of LPC with depth, lateral location, and percentage shortening; and (3) estimate the effect of lithology on LPC.

During progressive deformation, a modeled accretionary wedge, which formed during the shortening of the models, did not undergo homogeneous compaction; instead, loss of area varied in both space (with depth and laterally) and time. Balancing the area of sequential sections of one of the sand models, which was shortened above a high-friction

[1]*Present address*: BP Trinidad and Tobago LLC, Queens Park Plaza, Port of Spain, Trinidad and Tobago, W.I.

basal dêcollement, shows that the layers experienced tectonic compaction during deformation and lost as much as 17% of their cross-sectional area during 50% bulk shortening.

Restoration of two model profiles shows that LPC is three times greater in the model with high basal friction than in the model with low basal friction. In models where a sand layer was embedded within a viscous layer (a Newtonian material simulating rock salt), the layer accommodated all the shortening by folding and underwent no significant LPC.

Examples from the Spanish Pyrenees are used to illustrate the significance of LPS in restoring profiles of contractional areas. In the eastern Spanish Pyrenees, on the basis of deformed raindrop marks and burrows, from 16 to 23% of total shortening is estimated to be by LPS, whereas only 6 to 10% of the total shortening is accommodated by folding.

Model results illustrate the lateral and temporal variations of penetrative strain within shortened layers. Outlining this heterogeneous distribution of penetrative strain and any associated volume loss is important in distinguishing areas of reduced porosity, which are significant for hydrocarbon exploration.

INTRODUCTION

Bed length measurement and area balancing are two effective tools for interpreting the deformation history and determining the amount of shortening in cross sections of contractional areas (Dahlstrom, 1969; Hossack, 1979; Dixon, 1982; Cooper et al., 1983; Woodward et al., 1985, 1986, 1989; Suppe, 1985; Ramsay and Huber, 1987; Baker et al., 1988; Marshak and Woodward, 1988; Moretti et al., 1990; Mitra, 1978b, 1994; Jaswal et al., 1997; Meigs et al., 1996; Mukul and Mitra, 1998). In most applications, either the length or the area of the shortened layers is kept constant during reconstruction of the balanced cross sections.

Deformation in fold-and-thrust belts is accommodated by three main components: layer-parallel shortening, folding, and thrusting. If bed lengths are kept constant between the deformed and restored sections, one only accounts for deformation by folding and thrusting, so that layer-parallel shortening is not considered when the amount of bulk shortening is quantified. If strain markers are available, penetrative strain can be included in the balanced cross sections to restore the amount of shortening (Hossack, 1978; Mitra, 1990; Protzman and Mitra, 1990; Howard, 1993; Homza and Wallace, 1997).

Using examples from the Norwegian Caledonides, Hossack (1979) emphasized the necessity of areal restorations and pointed out possible errors that may be introduced if area decreased during shortening. Fischer and Coward (1982) quantified strain distribution in the Scottish Caledonides and concluded that prethrusting strain was not homogeneously distributed in the wedge. From deformed burrows, these authors measured a maximum local shortening of as much as 33%. In an excellent paper, Cooper et al. (1983) discussed the significance of layer-parallel shortening in balancing geologic cross sections and concluded that both bed length and area must be analyzed to recognize layer-parallel shortening. On the basis of stratal thickness calculations in a small-scale duplex in a limestone quarry, and assuming that area was conserved, Cooper et al. (1983) concluded that, in a total shortening of 49%, 27% was accommodated by LPS and the rest by imbrication.

Woodward et al. (1986) documented how strain varied in different thrust sheets in the southern Appalachians. In incompetent formations, they measured axial ratios of strain ellipse that increased, from external to internal thrust sheets, by $R = 1.2$ to $R = 2.8$.

In the shallow thrust system of the Oslo region, Morley (1986) recorded a maximum shortening by pressure solution of 15%, variably distributed within the belt. However, he suggested an average value of 5% for limestones across the entire section.

Mitra (1994) also emphasized the effects of LPS in thrust-belt restoration. In a regional cross section of the Sevier belt, he used different kinds of strain markers to show that LPS varies between 10 and 30% in the belt. McNaught and Mitra (1996) used finite strain data to document an LPS component of about 15% in the Meade thrust sheet of the Sevier Thrust Belt.

Because the initial stages of sand models are well documented, they are easy to compare with their later stages to quantify the components of strain. Many workers have used sand models to study different aspects of accretionary wedges and/or fold-and-thrust belts (Davis et al., 1983; Dahlen et al., 1984; Malavieille, 1984; Karig 1986; Zhao et al., 1986; Mulugeta and Koyi, 1987, 1992; Colletta et al., 1991; Liu et al., 1991; Koyi, 1995; Storti and McClay, 1995; Gutscher et al., 1996; Storti et al., 1997; Koyi et al., 2000; Lohrmann et al., 2003). In this study, layer-parallel compaction (LPC) is quantified in

five sand models, which have been shortened from one end, to comment on the distribution of layer-parallel shortening (LPS) and to illustrate the significance of area loss within accretionary prisms and fold-thrust belts. LPC is quantified by measuring the cross-sectional area of deformed layers and comparing them to their undeformed initial areas. In some models, bed length is restored to estimate amount of penetrative strain in comparison with the other components of shortening (imbrication and folding).

MODELS AND THEIR LIMITATIONS

We have quantified layer-parallel compaction (LPC) in five sand models with different initial configurations (Table 1). All models consisted of passively layered, loose sand and were shortened from one end. After the models were shortened, they were sectioned and photographed for analysis.

Dry, loose sand is a suitable material to simulate the brittle Coulomb behavior of shallow crustal rocks (Hubbert, 1937, 1951; Horsfield, 1977; McClay and Ellis, 1987; Ellis and McClay, 1988; Mandl, 1988; Mulugeta, 1988; Cobbold et al., 1989; Weijermars et al., 1993). Dry sand has a Navier-Coulomb rheology and an angle of friction similar to that of sedimentary rocks (cf. McClay, 1990). The rheology of loose sand may be approximated by the Coulomb equation (Hubbert, 1937; Cobbold et al., 1989; Weijermars et al., 1993):

$$\tau = \tau_o + \sigma \tan \phi \qquad (1)$$

where τ is the shear strength, τ_o is the cohesive strength, σ is the normal stress, and ϕ is the angle of internal friction. For the material used in the models, the cohesive strength, and the angle of internal friction, see Table 1.

This study is a two-dimensional approach that assumes no movement along strike, because movement perpendicular to transport direction is significantly small relative to movement parallel to it. In this experimental approach, we have omitted the additional complicating factors of erosion, deposition, material anisotropy resulting from facies changes, and time variations in pore-fluid pressure ratios across the wedge. All the models were deformed on a rigid horizontal planar substrate and therefore do not account for slopes or irregularities in natural dêcollements. Model 4 was shortened above a ductile substrate of a Newtonian silicone polymer (SGM36; Weijermars et al., 1993) that simulated rock salt or overpressured shale. In the description of the models, these variations are distinguished. Because gravity compaction is minimal in sand models, lateral compaction in full-scale prisms can be overestimated. In general, penetrative strain in a rock unit is strongly dependent on lithology, temperature, and fluid content. In our models, we have quantified LPC as a representative of penetrative strain. The effects of temperature and fluid content are not taken into account in the models. However, in one of the models (model 3), materials with different mechanical properties are used to study the influence of lithology on the amount and distribution of LPC.

To estimate the amount of layer-parallel compaction in the models, the shortening that results from thrusting and folding of each layer was restored. The resulting bed-length was compared with the initial, known length of the layers. The difference between the two lengths gave the amount of layer shortening (bed-length change) without taking the thickening of the layer into account. However, during restoration, most of the shortening is not accompanied by thickening of the layers, but is instead accompanied by an area loss. Hence, it can be described as layer-parallel compaction (LPC). Area loss was calculated by comparing the area in a profile of the deformed model with the area in a profile in the undeformed, initial stage.

LAYER-PARALLEL COMPACTION IN THE MODELS' THRUST WEDGES

During compression, a layer can accommodate the shortening in three ways: by layer-parallel shortening

Table 1. Mechanical properties of materials used, and dimensions of, the five models.

Model	*Thickness (cm)*	*Nature of detachment*	*Coefficient of internal friction /viscosity*	*% Bulk shortening*
1	0.7	frictional	loose sand (0.57)	47
2	1.5	frictional	loose sand (0.57)	20
3	2.5	frictional	glass beads (0.37)	27
4	2	frictional/viscous	loose sand (0.57)/ SGM36 (5×10^4 Pa s)	35
5	3.5	frictional	loose sand (0.57)	21

(LPS), folding, or thrusting. However, the intensity and amount of shortening accommodated in each way depend on the mechanical properties of the layer and its surrounding host, and on the boundary conditions. In many natural cases, three internal deformation mechanisms are common to the emplacement of imbricate sheets. An initial phase of layer-parallel shortening precedes or is simultaneous with propagation of the sole thrust (Cooper et al., 1983; Williams and Chapman, 1983; Marshak and Engelder, 1985; Nickelsen, 1986; Geiser, 1988a, b; Evans and Dunne, 1991). Next, a second phase of non-layer-parallel shortening and bending strain occurs (Wiltschko, 1981; Sanderson, 1982; Suppe, 1983; Kilsdonk and Wiltschko, 1988). Finally, there is a later phase of pure-shear shortening and simple shear (parallel to the sole thrust) that accompany the thrust-sheet transport (Elliot, 1976; Mitra and Elliott, 1980; Coward and Kim, 1981; Sanderson, 1982). In most natural examples, it is relatively easy to determine the amount of shortening that occurs by folding and thrusting. In the presence of appropriate strain markers, it is also easy to determine penetrative strain and LPS. However, on seismic profiles, unlike the folding and thrusting components, layer-parallel shortening is more difficult to estimate. Layer-parallel shortening can be accommodated by plastic deformation of mineral grains and formation of fabric, reduction of porosity (secondary or tectonic compaction), and by dissolution of minerals (for example, formation of stylolites). To address the penetrative strain in the Appalachian orogenic belt, Mitra (1978a) described regional variations in deformation mechanisms (e.g., pressure solution, dislocation creep, and grain boundary sliding) that affect sandstones and quartzites in that area. Penetrative strain, as a general phenomenon during the evolution of fold-and-thrust belts, has been described and quantified by many workers (Helmstedt and Greggs, 1980; Mitra et al., 1984; Geiser, 1988a, b; Mitra, 1988; Protzman and Mitra, 1990; Evans and Dunne, 1991; Gary and Mitra, 1993; Howard, 1993; Thorbjornsen and Dunne, 1997; and others).

Unlike in nature, in a model it is easy to estimate layer-parallel penetrative strain by comparing the initial and final stages of that model. Each of the five models described in this chapter studies one element that influences the amount or distribution of LPC within a model fold-and-thrust belt. We show here that, at any given stage of model deformation, area loss is not constant. It varies laterally and with depth, amount of bulk shortening, and material properties.

Variation of LPC with Depth

Model 1, which was used to study the variation of LPC with depth, contained passively colored homogeneous sand with a constant total thickness of 5 mm (Mulugeta and Koyi, 1992; Koyi, 2000). Sequential sections were eroded using a vacuum cleaner, and then photographed, at every 1.5% increment of bulk shortening. This technique exposed the three-dimensional geometry of the imbricate sheets, so that fine-grained sand and thin (0.2-mm-thick) individual sand layers could be used to quantify area loss and penetrative strain. The model was shortened to a total of 47% bulk shortening (Figure 1). For more details of deformation and sectioning of this model, see Koyi (1995).

In a profile of the final stage of the deformed model, bed-length restoration was conducted for three layers located at different stratigraphic horizons (Figure 2). Bed-length restoration was used to partition the amount of deformation accommodated by each of the three strain components: layer-parallel compaction, folding, and thrusting. The effects of imbrication and folding were removed by measuring the segment length of each deformed layer and adding them together. By comparing this ''restored'' length with the deformed length, the amount of shortening by imbrication and folding was calculated. This restored length was then compared with the initial (undeformed) length of the model to calculate the amount of shortening accommodated by layer-parallel compaction. In all the cases, the restored length of the beds was shorter than their initial length (Figure 2).

To quantify the change in the mode of deformation with depth, longitudinal strain was partitioned into three layers located at different stratigraphic levels (top, middle, and bottom) (Figure 2). Earlier, Koyi (1995, 2000) had documented that layer-parallel compaction dominates in deeper levels of model accretionary

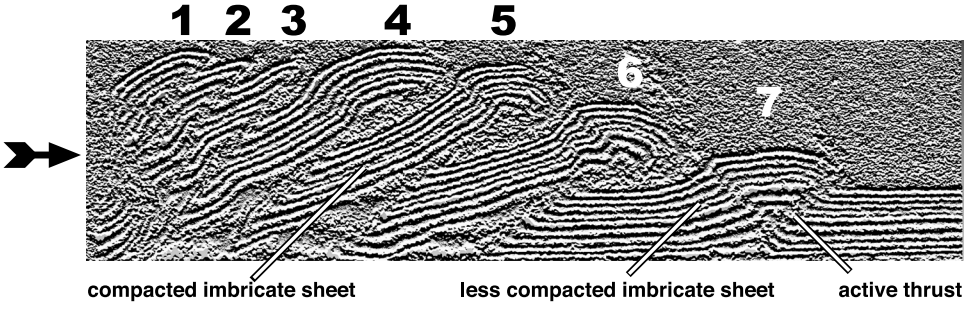

FIGURE 1. A relief image of a profile of model 1 after 40% shortening, showing seven imbricate sheets. The numbers indicate the sequence in which the imbricates have formed. Arrow shows direction of shortening.

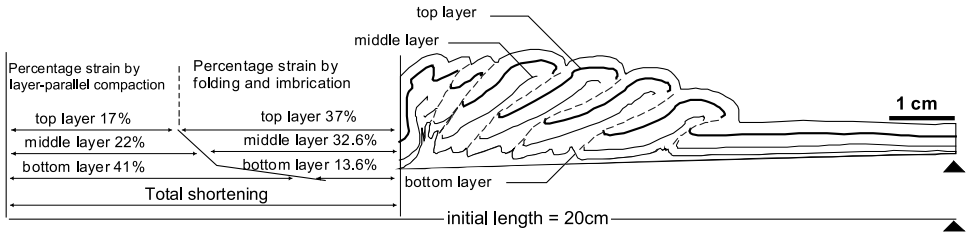

FIGURE 2. A line drawing of a profile of model 1 at 44% bulk shortening. Three layers (top, middle, and bottom) are restored to quantify the three components of shortening (layer-parallel shortening, folding, and imbrication). Note that the top layer deforms mainly by folding and imbrication, in contrast to the bottom layer, which deforms mainly by layer-parallel thickening.

wedges, whereas imbrication prevails at shallower levels. The current analysis demonstrates that the shallow (top) layer could be restored back to 83% of its initial length (Figure 2). The remaining 17% of the initial length, which was not restorable, was consumed by layer-parallel compaction during deformation of the model. This latter strain component was recoverable in the model because its initial dimensions were known. The deep layer, on the other hand, could only be restored to 59% of its initial length (Figure 2). In this layer, the entire remaining (unrestored) 41% of the layer length was consumed by layer-parallel compaction. This comparison illustrates that the mode of deformation within a modeled imbricate stack changes with depth. It also points out that balancing the bed lengths of different layers in natural profiles of shortened areas may yield different percentages of shortening. Because, in the absence of a good estimate of LPC, deeper layers are restored to shorter initial lengths than are shallower layers; they show a higher percentage of bulk shortening.

Lateral Variation of LPC

Model 1 was also used to quantify the lateral change in the amount of penetrative shortening. In this model, the area of an imbricate (in this case, imbricate number 4) was measured at the onset of its formation (and throughout its deformation) until a new imbricate (number 5) formed in front of it. During the same time interval, the area of the model wedge was measured to compare loss of area within the wedge and the imbricate during the same period of deformation (Figure 3).

Restoration of the model wedge between two stages of imbricate formation shows that 76% of the total area lost within the wedge was accommodated within the youngest of the imbricates at the toe (Figure 3). During the same period of deformation, the entire wedge lost only 3.9% of its area, of which 3% was accommodated by the youngest of the imbricates. This imbricate sheet lost 10.5% of its initial area during the same period of deformation (Figure 3). These results suggest that the newly accreted materials at the toe of the wedge underwent secondary tectonic compaction, whereas the rear part of the wedge, which contained an older stack of imbricate sheets and was already strongly compacted, could not accommodate much more tectonic compaction with deformation. In general, cumulative compaction was highest at the rear of the wedge, whereas incremental compaction was highest at the toe area. In other words, as the wedge grows, incremental compaction localizes within the newly accreted material at the toe of the model. The rear portion of the wedge is transported almost as a rigid block, without much strain, while the wedge accretes material at the toe. Naturally, synkinematic erosion or any change in the basal slope or friction may relocate the deformation and thereby alter this scenario.

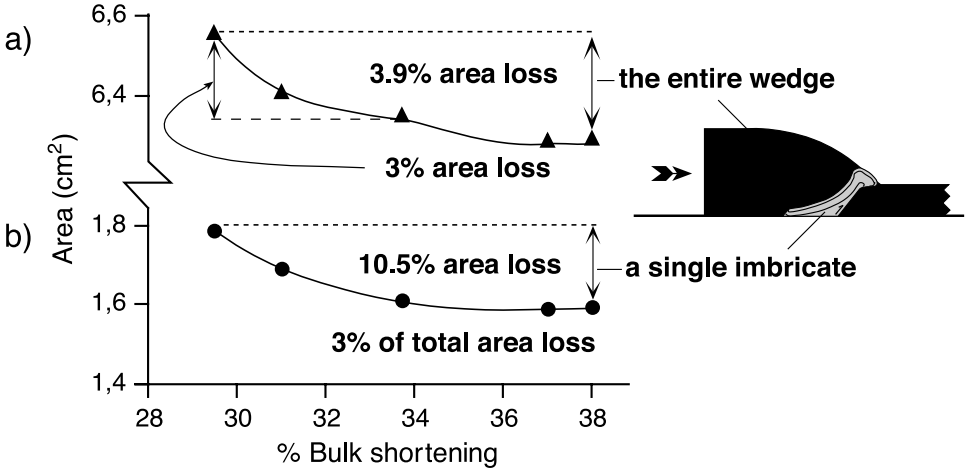

FIGURE 3. Plots of (a) wedge area (triangles) and (b) imbricate area (circles) versus bulk shortening of model 1. At 38% shortening, the wedge loses approximately 4% of its initial area. During the same period, the youngest imbricate loses 10.5% of its initial area, which is equal to approximately 3% of the total area of the wedge. This suggests that much of the area lost within the wedge is accommodated within the youngest imbricates at the toe.

Change of LPC with Percentage of Bulk Shortening and with Material Properties

Model 2 was used to illustrate how the penetrative strain varies with the amount of bulk shortening. In this model, LPC was measured for two layers located at different stratigraphic levels in two sections shortened to different percentages of bulk shortening (Figure 4). As expected, LPC increased with increasing percentage of bulk shortening. However, there was a significant difference in the change in LPC between the two layers (Figure 4). At 5% bulk shortening, the shallow layer accommodated only 1% of the bulk shortening by LPC, whereas at 20% bulk shortening, LPC in the same layer was seven times greater (7%). The difference in LPC in the deeper layer between two stages of bulk shortening was only fourfold. Comparing the area of the initial stage of the model with its area at the final stage of deformation shows that there is an area loss of 1% at 5% bulk shortening and a loss of 4% at 20% bulk shortening (Figure 5).

To quantify the change in LPC with lithology, model 3 was prepared using two materials with different mechanical properties: loose sand and glass beads. This model was shortened to 27% bulk shortening. To simulate a rock that does not undergo much compaction during shortening, we used a layer of well-sorted glass beads, which as a medium is mechanically weaker [has a lower coefficient of internal friction (0.37)] than loose sand used in our models. This model consisted of a 4-mm-thick layer of beads overlain by three layers of loose sand, each of which were 5 mm thick. The model was shortened from one end to a total shortening of 27%. A section of this model was area-balanced to measure the amount of area lost in each layer (Figure 5). The analysis showed that the glass-bead layer preserved its cross-sectional area and underwent no significant amount of LPC, although it was located at deeper levels, where penetrative strain is usually dominant in other models such as models 1 and 2 (Figure 5). Instead, the glass-beads layer accommodated the bulk shortening by layer-parallel thickening. The sand layers, on the other hand, underwent different amounts of LPC. The deeper layer lost 5% of its area, whereas the shallow layer showed an area loss of only 1.5%. This demonstrates that the area lost in different lithologies is accommodated differently depending on how each lithology compacts.

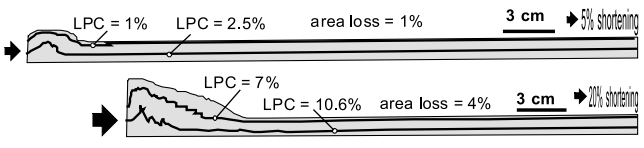

FIGURE 4. Line drawings of two profiles of model 2 at two different percentages of bulk shortening. As expected, LPC increases with the increase of the amount of bulk shortening and with depth.

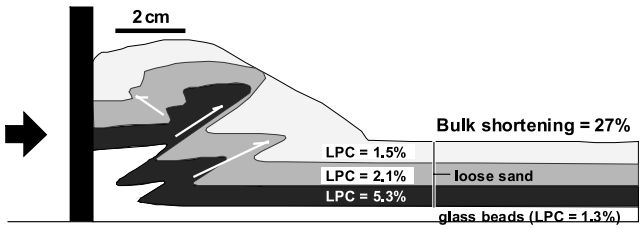

FIGURE 5. Line drawing of a profile of model 3, consisting of layers of loose sand overlying a layer of mechanically weaker glass beads. The layer of beads undergoes significantly less LPC than do the sand layers, but thickens instead.

Oblique Sections

For us to achieve a correct restoration, we need for the section to be parallel or nearly parallel to the transport direction. This is because a profile that is oblique to the shortening direction is naturally longer than profiles parallel to the shortening direction; hence, it is expected to have a longer initial bed length. Many times, only oblique profiles (profiles not parallel to the shortening direction) are available, and some workers apply the restoration technique to available seismic profiles even though they are not parallel to the shortening direction. Recently, Jaswal et al. (1997) restored a composite seismic image across the north Potwar deformation zone (NPDZ) and Dhurnal structure of the Himalayan foreland of Pakistan. The seismic image consisted of three segments: a northern north-south segment parallel to the shortening direction, a middle segment making an angle of 30° with the northern segment (but at a high angle to the structures), and a southern segment making an angle of 40° with the northern segment. By balancing this composite section, Jaswal et al. (1997) suggested a minimum amount of shortening across the NPDZ to be more than 55 km, at a rate of 18 mm/yr. Wissinger et al. (1998) conducted a similar exercise on a reflection seismic line that was oblique by 55 to 60° to the strike of the thrusts in the central Brooks Range in Arctic Alaska. Wissinger et al. (1998) restored the deeper structures and estimated a minimum shortening of 500 to 600 km in the Brooks Range. Price (1981) stated that the amount of tectonic shortening can be estimated from sections that make an angle of less than 30° with the actual direction of net tectonic displacement. According to Cooper (1983), a 20° obliquity between the balanced section and the transport direction will not greatly affect bulk-strain calculations on the balanced section of the structures.

Below, we restore a model profile that is oblique to the direction of shortening. We compare it with a

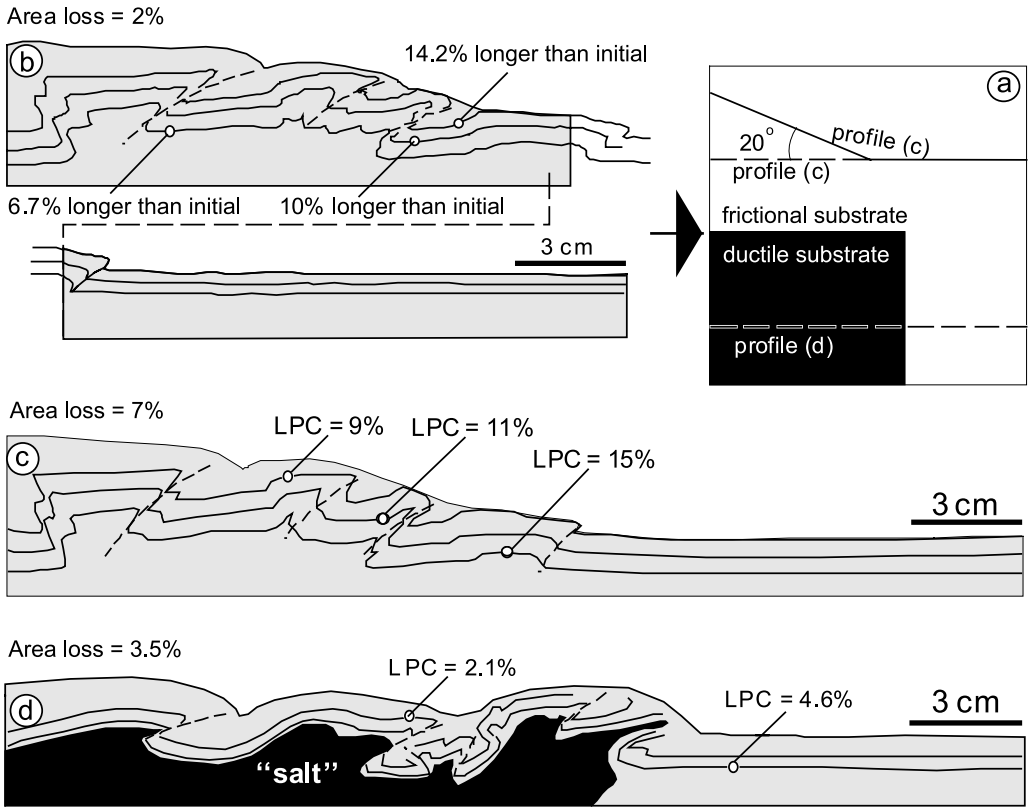

FIGURE 6. (a) A schematic diagram of model 4 in plan view, showing the locations of three profiles (b, c, and d) cut in the two domains (frictional and viscous substrates) for restoration after 35% bulk shortening of the model. (b) Line drawing of a profile, cut in the frictional-substrate domain, consisting of two segments (a rear segment oblique to shortening direction and a frontal segment parallel to the shortening direction). Note that after restoration, the layers in this profile are longer than the initial length of layers in a profile parallel to transport direction (see c). (c) Line drawing of a profile in the frictional-substrate domain cut parallel to the shortening direction. The layers in this profile have undergone LPC and therefore cannot be restored to their initial length. Note that the deeper layers undergo more LPC than the shallow layers do. (d) Line drawing of a profile cut in the viscous-substrate domain. LPC shortening in these layers is significantly less than their equivalents shortened above a frictional substrate in (c).

restored profile cut parallel to the shortening direction and illustrate the discrepancy that can result from restoring oblique sections.

In model 4, we studied the role of frictional and viscous (salt) dêcollements in governing deformation style. In this model, a package of layers of loose sand was deformed: one half was shortened on another sand layer and the second half was shortened above a viscous layer (SGM36, a Newtonian viscous material) (Figure 6a). This model simulated the deformation history of the Potwar and Salt Range of Pakistan (Cotton and Koyi, 2000). Here, we use the model to illustrate (1) the effect of restoration of oblique sections (those not parallel to the transport direction; Figure 6b), and (2) the effect of a ductile substrate on the mode of deformation and amount of penetrative strain within the overlying units (Figure 6d). As with the other models, this model was shortened from one end. After 35% shortening, three profiles were prepared for restoration (Figure 6). Two profiles were cut parallel to the shortening direction: one in the viscous substrate domain and the other in the frictional-substrate domain (Figure 6c and d). The third profile was a composite section consisting of two segments: a segment making an angle of 30° with the shortening direction, and a second segment parallel to the shortening direction (Figure 6b). All three profiles were restored and compared with the initial stage of the model to calculate the penetrative strain accommodated by layer-parallel compaction (Figure 6). Results for the parallel profile cut in the frictional domain were similar to those for other models, in which layer-parallel compaction increased with depth (Figure 6c). In this profile, a deep layer accommodated 15% of the shortening by penetrative strain, compared with 9% for a shallow layer (Figure 6c). The composite section, cut in the frictional-substrate domain, showed totally different results. After restoration, the layers in this section, as expected, were longer than the initial length of the layers in the section that was parallel to the shortening direction. The shallow layer was 14% longer, whereas the deep layer was 6.7% longer than the initial layer (Figure 6b). The amount of shortening in this

section differs from that in the section cut parallel to the shortening direction by approximately 25%. This difference is because the composite section, which consists of a segment oblique to the shortening direction, is initially longer than any section parallel to the shortening direction. Hence, its restored version does not display the correct amount of shortening.

The area of each section is compared with the area of an undeformed section. The parallel profile showed an area loss of 7% (Figure 6c). The oblique section, however, showed a very small amount of area loss (2%, Figure 6b). This discrepancy is because this section is oblique to the transport direction and hence shows a larger initial area. These results demonstrate quantitatively that neither bed length nor area balancing of oblique sections gives the correct amount of bulk shortening.

Change of LPC and LPS with Basal Friction

In model 4, a section that had been cut in the viscous substrate domain was restored and compared with its initial stage to estimate the amount of LPC with depth (Figure 6d). Here, the amount of deformation accommodated by LPC, even at the deeper levels, was significantly smaller (Figure 6d). In the deeper layer, only 5.6% of the deformation was accommodated by penetrative strain, compared with 2% for the shallow layers. Compared with the section cut in the frictional substrate domain (where LPC was 15% for the deeper layer and 9% for the shallow layer; Figure 6c), these figures suggest that layer-parallel shortening in the overlying sediments decreases significantly in the presence of a viscous substrate. This is because the ductile layer decreases the friction along the basal dêcollement and eases forward propagation of the deformation front, instead of contributing to a wedge buildup.

In another model (model 5), which consisted of alternating sand and ductile layers, LPC within the layers varied significantly depending on the location of the sand layers relative to the ductile layers (Figure 7). In this model, alternating layers of loose sand and a viscous material (SGM36) were shortened, from one end, to 21% bulk shortening (Figure 7). During shortening, the sand layer, which was embedded between two viscous layers, underwent the least LPC. It is feasible that even that amount of LPC in this layer is accommodated mainly by the rear portion of the layer, which was not embedded between the viscous layers (Figure 7). Had the entire layer been embedded between the two viscous layers, it would have accommodated the shortening only by folding. In this model, a deeper layer underlying the two viscous layers underwent more LPC than the other layers (Figure 7). This model reemphasizes how significant the presence of a viscous layer is in partitioning strain within nonevaporitic frictional sediments. Because a viscous substrate flows easier than the rest of the model, it provides a low basal friction, which allows the sole thrust to propagate farther without the necessity of building a steep wedge. The low tapered wedge therefore undergoes less internal compaction and hence less penetrative strain and LPC.

NATURAL EXAMPLES

Two examples from the Pyrenean orogenic belt are discussed here to illustrate the significance of LPS: the Pyrenean hinterland and the south-central Pyrenean Fold-and-thrust Belt.

Pyrenean Hinterland

The structures of the Pyrenean hinterland consist of an Alpine antiformal stack involving mainly Paleozoic rocks and a Mesozoic-Cenozoic cover (Teixell, 1996; Teixell and Koyi, 2003). These rocks were deformed during the Hercynian orogeny. In the western Axial Zone, the Mesozoic-Cenozoic sediments, which from bottom to top consist of Upper Cretaceous carbonates, calcareous shale, Marbore Sandstone, Paleocene limestone, and Eocene turbidites, form an imbricate stack verging to the south. In this area, with its good exposure, it is relatively easy to estimate the amount of shortening accommodated by thrusting and folding

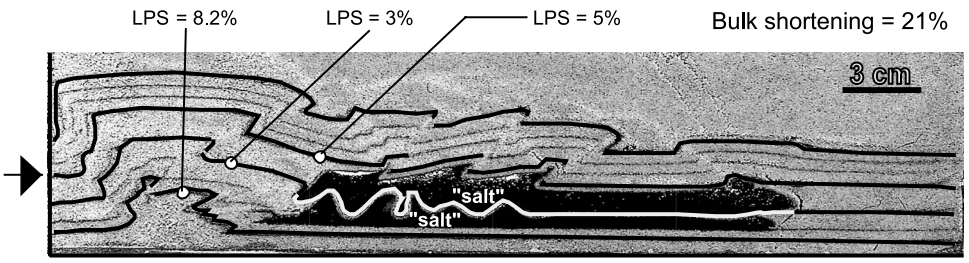

FIGURE 7. Photograph of a profile of model 5, consisting of two viscous layers simulating salt embedded between layers of loose sand. This model was shortened by as much as 21%. The three layers outlined on the profile have undergone different amounts of layer-parallel compaction (LPC), depending on their stratigraphic location and their relation to the viscous layers. The middle layer, which is embedded between the two viscous layers, has undergone the least LPC, because it accommodated most of the deformation by folding. The deepest layer has undergone the maximum amount of LPC.

(a)

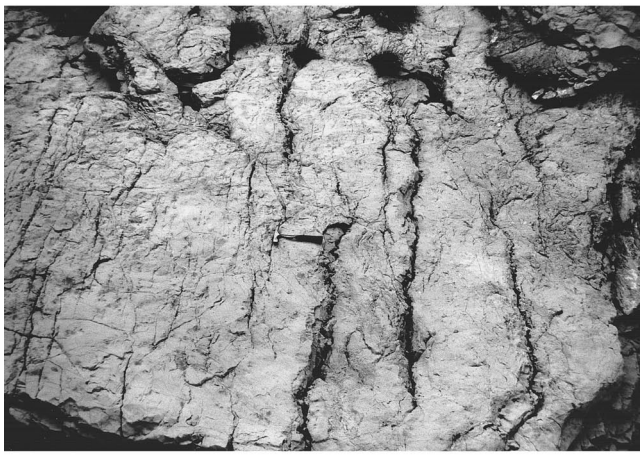

(b)

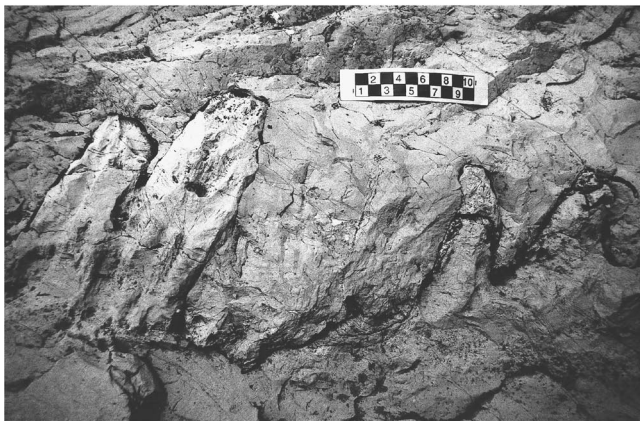

FIGURE 8. (a) An oblique photograph of the bedding plane of a limestone layer of the Pyrenean hinterland (Paleocene cover of the western Axial Zone), showing stylolites normal to the bedding. (b) Photograph of a profile of a limestone layer showing stylolite peaks oblique to bedding (horizontal). Note the inclined peaks of the stylolites, which make an angle of 60° with the bedding.

(Teixell and Koyi, 2003). Evidence for penetrative strain is visible in all the units and positions, in addition to the fold forelimb regions, which show a strong heterogeneous strain (Alonso and Teixell, 1992). The turbidites and the sandstone units show a northerly dipping tectonic fabric that is especially well developed in the turbidites. The carbonates, on the other hand, have not developed any visible cleavage, but show two kinds of stylolite joints: a set perpendicular to bedding and another set parallel to bedding (Figures 8a, 8b, and 9). The bedding-perpendicular stylolite joints are interpreted to have formed during early stages of layer-parallel shortening, when the carbonates were deformed by penetrative strain before folding and imbrication (Figure 9). The teeth in these stylolite joints are typically smaller (<1 cm) (Figure 8a). Evans and Dunne (1991) recorded meso-scale bed-perpendicular stylolites in the North Mountain thrust sheet of the central Appalachians and also interpreted them as evidence for an early layer-parallel shortening event. The bedding-parallel stylolite joints, on the other hand, are accompanied by vertical calcite veins and are interpreted to have formed as a result of tectonic loading by older overlying imbricates (Figure 9). The teeth of these joints are significantly larger (up to 10 cm) and are dipping in the direction of transport (Figures 8b and 9). Only the normal set formed by layer-parallel lateral shortening (Figures 8a and 9). These structures indicate that all units in the Pyrenean alpine hinterland have accommodated part of their deformation by penetrative strain. In the absence of systematic quantitative indicators, not accounting for penetrative strain will result in only a partial restoration of the deformation.

The South-central Pyrenean External Fold-and-thrust Belt

Calculating the amount of layer-parallel shortening in the external areas of a fold-and-thrust belt usually is not an easy exercise. In the south Pyrenees, different techniques, such as analysis of the strain markers, fissility ratios, and anisotropy of the magnetic susceptibility have been used to estimate layer-parallel shortening in several traverses (Casas et al., 1996; Sans, 1999). Here, we will discuss the results of the analysis of the sedimentary strain markers along the Cardener River traverse to quantify layer-parallel shortening in the deformed south Pyrenean foreland.

The south Pyrenean front developed a triangle zone that coincides with the presence of three partially superposed evaporitic levels at depth (Vergés, 1993; Sans et al., 1996). This triangle zone widened as successive thrusts that developed at the pinch-out of each evaporitic formation front (Beuda, Cardona, and Barbastro) were abandoned and the sole detachment climbed from

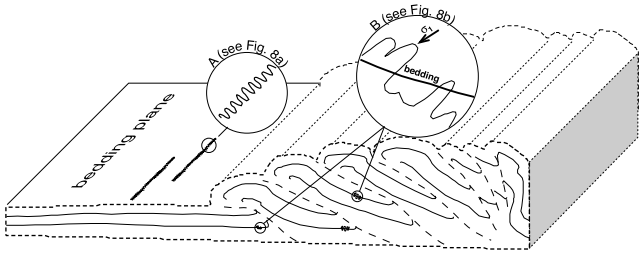

FIGURE 9. Schematic line drawing showing the location of the two sets of stylolites observed in the Pyrenean carbonates. Set (A), which is normal to bedding, is interpreted to have formed as a result of layer-parallel shortening before folding and imbrication, whereas set (B) formed as a result of tectonic loading of older imbricates.

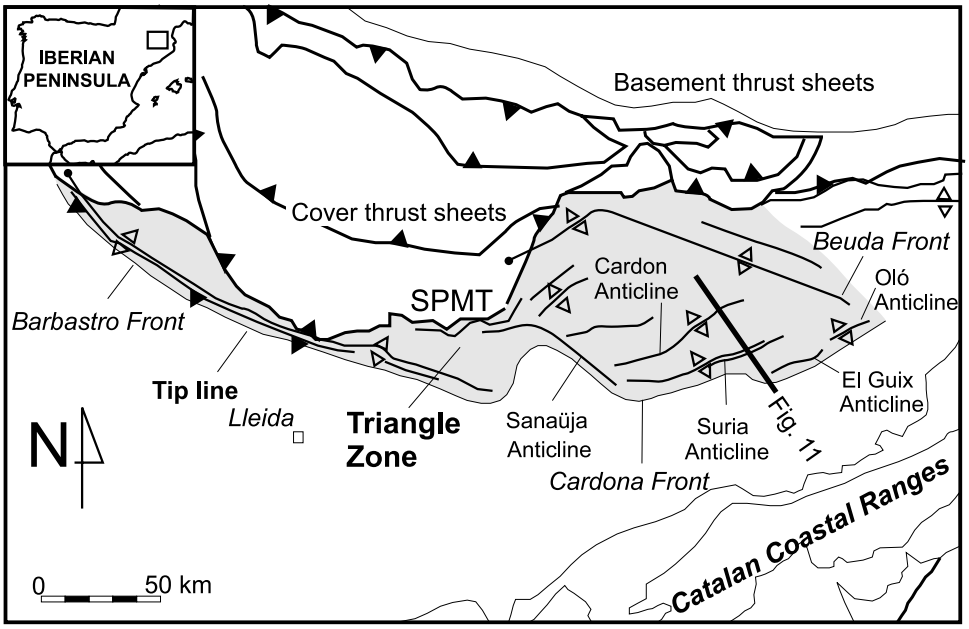

FIGURE 10. Map of the south Pyrenean triangle zone. Inset shows the Iberian Peninsula and location of the study area in the Pyrenees. The black bar shows the sampled section across the Cardona front, from under the detachment horizon to the Cardona Anticline. SPMT stands for South Pyrenean Main Thrust.

lower evaporitic formations in the north to higher ones in the south (Figure 10). In order to quantify LPS, we have analyzed samples from different parts of this area. Samples were collected in a north-south section that crosses the Cardona thrust front (Figures 10 and 11). The southernmost samples were collected from below the detachment level (Cardona salt formation), whereas to the north, three different anticlines above this detachment horizon were sampled. The three structures sampled are, from south to north, the El Guix Anticline, the Suria Anticline, and the Pinós-Cardona Anticline (Figure 11). The El Guix and Suria Anticlines are the frontal structures in the southeastern part of the thrust front (Figure 10). Both of these anticlines have a thrust-wedge geometry characterized by a north-verging structure in the south and a south-verging structure in the north separated by a narrow syncline (Figure 11). The Cardona Anticline (Figure 11) is a south-verging detachment anticline developed where the Cardona salt is thickest (center of the evaporitic basin).

The preserved sedimentary pile is less than 500 m thick in the frontal thrust-wedge (El Guix Anticline) and more than 2 km thick in the northernmost syncline (north of the Cardona Anticline). The scarce vitrinite analysis in the basin indicates, however, that there was a sedimentary thickness of approximately 2.5 km over the Cardona salt at El Guix Anticline (Vergés et al., 1998). These data are consistent with the preserved sedimentary thickness in the northern syncline and the small (<0.5°) sedimentary slope of the deformed sediments (Sáez, 1987). The sampled sediments are fine-grained red and gray sandstones that contain burrows

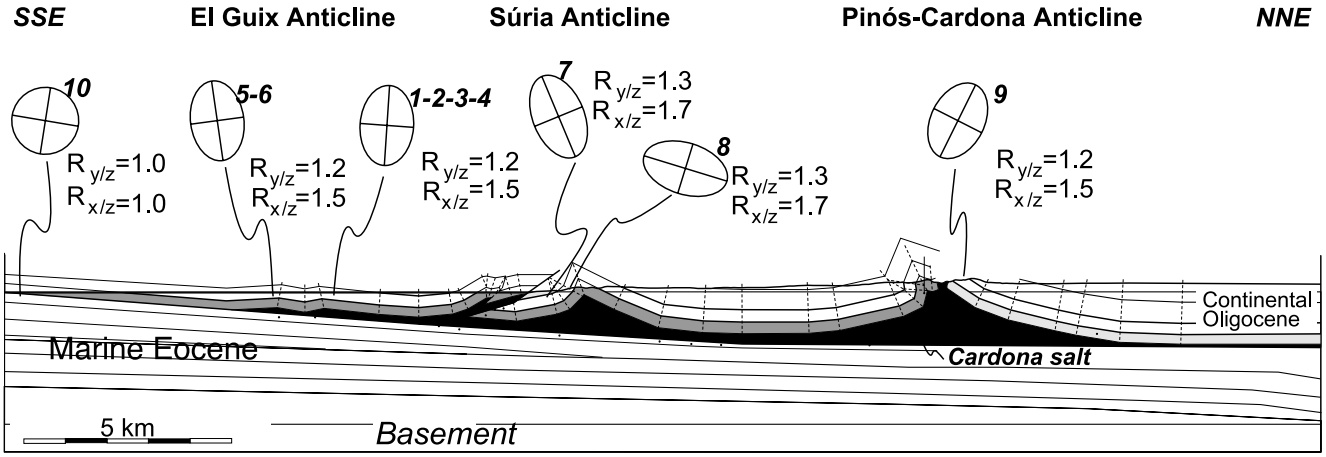

FIGURE 11. Regional section of the Cardona thrust front. Ellipses show the *Z*/*X* section of the strain ellipsoid. Numerical values show the ellipticity (R = *y*/*z*) of the *y*/*z* section measured on the bedding plane, and the ellipticity in the *x*/*z* plane (R = *x*/*z*) calculated for the vertical section. Ellipses of locations 1, 2, 3, 4, and 5 are projected along strike from the eastern section. Ellipses from locations 6, 7, 8, 9, and 10 lie in the plane of the section.

Table 2. Ellipticity (R) and orientation (φ) values of the strain ellipses in the Cardona thrust front.

Location	*No. of samples*	*Marker type*	*R*	ϕ	*No. of measurements*
		El Guix- Sallent			
1	1	Burrows	1.2	73	12
2	8	Burrows Oxidation marks Rain drops	1.2	71	186
3	3	Burrows	1.2	78	76
4	1	Burrows	1.2	72	14
5	2	Burrows	1.2		104
		El Guix- Callús			
6	1	Burrows	1.2		27
		Súria			
7	1	Burrows	1.3	47	10
8	2	Burrows	1.3	47	10
		Cardona			
9	4	Burrows	1.2	62	102
		Manresa			
10	3	Burrows	1.0		56

and other strain markers. These sediments belong to the alluvial/fluvial and lacustrine sequences that filled the south-Pyrenean foreland basin. Although the sampled levels are not the same through the whole structure, the samples have been collected from an interval of 500 to 800 m from the top of the salt, and the estimated age for these sediments is early Oligocene.

Sampling is irregularly distributed through the structures, because the presence of strain markers is highly dependent on lithology. The frontal thrust wedge (El Guix Anticline) was profusely sampled, especially in the north (1 sample every 25 m), whereas no strain markers have been found in the central syncline (Figure 11). The El Guix Anticline was also sampled 10 km to the west (Figure 10), in younger sediments (1000 m above the top of the salt). The Súria Anticline was sampled in the footwall of the main back thrust, and the Cardona Anticline was sampled in the northern limb of the anticline (Figure 11).

The oriented samples were photographed and drawn for analysis by the IMAT program developed by the Serveis Cientifico-Tecnics of the Universitat de Barcelona (Durney, 1995). This program analyzes the image and determines the long and short axes, the area and the perimeter of the strain marker, and orientation of the long axis with respect to a reference line. These data are then processed by the GRFRFP program, developed at Barcelona University (Durney, 1995), which calculates the mean elongation value (Rf) and orientation (φ) by interactive retrodeformation of the set of ellipses to an isotropic distribution (where ln (Rf)/2ϕ vector mean is equal to zero).

The results presented here will be grouped in structural localities, which are separated by main thrusts or structural elements (Table 2 and Figure 11). To quantify penetrative strain, the *Z* axis is assumed to be contained in the bedding planes, because incipient cleavage is normal to bedding (Sans and Vergés, 1995). Also, a plane strain value is assumed for the area ($Y = 1$). This assumption is based on (1) lack of extensional structures perpendicular to the folds along strike; (2) absence of folds in the salt layer along strike that would indicate flow of the salt in a direction different from the overburden transport direction; and (3) minimum deformation of the halite grain shape (strain markers) in a section perpendicular to the shortening direction (Miralles, 1999).

The calculated ellipticity of the strain ellipsoid in the *YZ* section (bedding plane, Table 2) changes from 1.0 below the detachment to 1.2/1.3 above the detachment. This indicates the effective decoupling achieved by the Cardona salt formation. In contrast, there is no significant increase in ellipticity across the frontal thrust wedge, where the ellipticity is R = 1.2 in all the sampled localities—even in those measured along strike in a stratigraphically different position. There is also no significant increase between the frontal thrust wedge and the northernmost anticline located 30 km to the north. There is a slight increase in the Súria Anticline, where the samples were collected very close to the main back thrust. The deformation of these strain ellipses was achieved before folding and thrusting, because after unfolding, the strain ellipses in neighboring localities have the same orientation and values in beds that are

horizontal as they have in vertical or inclined beds. The orientation of the strain ellipsoid has a good gathering in the three sampled anticlines (El Guix, Cardona, and Suria). The azimuth of the *Y* axis varies from N74 to N47 and N62, respectively. These orientations are parallel to the fold axes at the sampled localities. The change in orientation between the three different folds can also be seen in map view (Figure 10).

Layer-parallel shortening calculated from the elongation parameters suggests 16% penetrative strain in the frontal thrust wedge (El Guix Anticline) and the northern anticline (Cardona Anticline), and 23% in the Súria Anticline. In contrast, in the same section, shortening accommodated by folding and thrusting is 5–6% in the El Guix and Cardona Anticlines and 10% in the Suria Anticline.

DISCUSSION

Penetrative strain is a significant element of shortening in many fold-thrust belts (Mitra, 1988, 1990). In this chapter, we apply the results of sandbox models to quantify the relative amount and distribution of layer-parallel strain within a fold-thrust belt or an accretionary prism. We assume that the layer-parallel compaction (LPC) observed in the sandbox models (which usually show little bed thickening) corresponds in style to that part of layer-parallel shortening (LPS) which is not accommodated by thickening of sedimentary layers in nature. It is worthwhile to underline, however, that the amount of LPC observed in the models does not equate to the amount of LPS in a natural case. However, by monitoring LPC in the models, we assume that model results can illustrate the distribution and style of penetrative strain within areas that have undergone compressional tectonism.

In layers of loose sand, the amount of LPC depends on shape and size of the sand grains and the degree of sorting. The variation in LPC between different models in which different types of loose sand are used is therefore attributed to variations in these parameters. However, the variation in LPC within the same model (e.g., LPC variations with depth in models 1, 2, and 4) in which the same type of sand is used, cannot be attributed to these features, but must be the result of heterogeneous distribution of strain within the sedimentary pile of the model during its shortening.

In the sand layers of the models, penetrative strain is accommodated by compaction through volume loss and porosity reduction. In nature, as documented from many thrust belts, this secondary (tectonic) compaction is likely to be accommodated for by volume loss through pressure solution and porosity reduction, but much of the layer-parallel penetrative shortening involves layer thickening. Mitra's (1988) theoretical derivation of the relationship between finite strain and original and final porosity indicated that little porosity is preserved in rocks whose strain (R) exceeds 1.5.

Comparison of the restored length with the initial length of the shortened model layers overestimates the amount of shortening that results from LPC, because layer thickening is not accounted for. However, comparing the cross-sectional area between the deformed and the undeformed profiles accounts for any thickening of the layer during shortening. Then the correct amount of LPC can be estimated, because the decrease in the cross-sectional area in the deformed profile is attributed to layer-parallel compaction.

Layer-parallel compaction in our models, which were shortened above a frictional dêcollement, is concentrated in front of and at the leading edge of the deformation front, where relatively less-compacted sediments are accreted (Figure 3). This is similar to the deformation style observed in Nankai accretionary prism, where shortening of the soft sediments in the prism toe is pervasive and is not just accommodated by displacement along imbricate thrusts and shear bands (Karig and Lundberg, 1990). Similarly, the active toe area in the wedge of model 1 accommodated most of the penetrative strain that the wedge experienced (Figure 3).

Within the same model (model 4), bed-length restoration of a section shortened above a viscous substrate showed only 3.5% area loss, compared with 7% area loss in the section shortened above a viscous substrate (Figure 6c and d). This suggests that there may be relatively less LPS in layers shortened above a viscous substrate than in similar layers shortened above a frictional substrate. Therefore, LPS in lithologies deformed above, for example, a layer of salt, is expected to be relatively less than it would be if these units were deformed above a frictional substrate. This is supported by the fact that estimated LPS in the external areas of the Spanish Pyrenees, which are not shortened above a layer of salt, is greater (30%) compared with LPS (20%) in the areas shortened above a layer of salt.

However, the example of the Spanish Pyrenees shows that even in the presence of a salt layer, a considerable amount (about 20%), of penetrative strain may be recorded in the layers shortened above the salt. This relatively high amount of LPS above a ductile layer is attributed to the thickness of the viscous layer and its distribution. A thin ductile layer, whose viscous flow is retarded by viscous drag, promotes more penetrative strain in the overlying units than a thicker viscous layer, which flows more easily. Before overcoming the basal friction, early shortening is partly consumed by penetrative strain within the layers. Hence, penetrative strain would be more effective.

The variation of strain with different modeling materials shown in model 3 could be applied to natural

cases where incompetent lithologies undergo more penetrative strain than do more competent units. A good example of this is given in the North Mountain thrust sheet of the central Appalachians, where the incompetent Ordovician Martinsburg Formation shows significantly greater strain (primarily plane strain) than do the more competent carbonates of the same thrust sheet (Woodward et al., 1986).

The effects of LPS must also be taken into account when one is interpreting porosity or sonic-velocity profiles in terms of apparent exhumation. In many inverted sedimentary basins (Bulat and Stoker, 1987; Menpes and Hillis, 1995; Tonghban, 2000) exceptionally high sonic velocities have been interpreted as remnants of earlier burial that has been removed by erosion. It is supposed that sedimentary rocks compact irreversibly when they are submitted to the pressure of overburden. This compaction decreases porosity and therefore increases sonic velocities. A comparison of velocity profiles in undisturbed and inverted basins allows us to model a minimum overpressure that the rock has suffered. This overpressure (P_o) can then be converted into minimum eroded overburden (h_o) using the formula $h_o = P_o/(g\rho)$, where g is the gravitational acceleration and ρ the mean density of the overburden.

In view of our results regarding LPS in shortened areas, this relationship should, however, be used with caution. Exhumation is certainly related to uplift. The uplift may be caused by deep processes, acting mainly vertically (e.g., heating of the lithosphere, or underplating), which will generally not increase the pressure in the overlying rocks by an important amount. However, in areas with significant horizontal shortening, inverted faults and thrusting would inevitably increase the pressure in the whole overthrust column. The horizontal force per unit length necessary to overcome gravitational and frictional forces along a thrust are given by the following formula (Turcotte and Schubert, 1982, p. 354):

$$F_x = \frac{f\rho g(1-\lambda)H^2}{\sin(2\beta) - f(1\ \cos(2\beta))} \qquad (2)$$

where f is the frictional coefficient (usually 0.7–0.85), ρ the average density of the hanging-wall rocks, g the gravitational acceleration, λ the pore pressure coefficient, H the thickness of the thrust sheet, and β the angle of the thrust fault with the horizontal.

The minimum force is necessary for an angle $\beta = 0.5*\arctan(1/f)$, giving

$$F_x = \frac{f\rho g(1-\lambda)H^2}{\sqrt{1+f^2} - f} \qquad (3)$$

The average tectonic stress amounts to $\sigma_{xx} = F_x/H$ and can be written as a function of the lithostatic pressure $P = \rho gH$ at the base of the thrust sheet:

$$\sigma_{xx} = \frac{f}{\sqrt{1+f^2} - f} * (1-\lambda) * P \qquad (4)$$

In situations of reasonable f and hydrostatic pore pressure, the average tectonic horizontal stress is between 50% and 100% of the lithostatic pressure at the base of the thrust sheet. Because this additional stress may increase the pressure by the same amount or more than would a possible eroded overburden, it is highly probable that exhumation estimates based on sonic velocity interpretations often are too large. In other words, in shortened or inverted areas, estimates of burial depth that are based on the compaction of units may be too high when the effect of horizontal compaction resulting from lateral shortening is not accounted for.

CONCLUSIONS

Analyses of sequential sections of sand models demonstrate the following.

1) Layer-parallel shortening, achieved mainly by layer-parallel compaction, is a significant component of deformation in sand models.
2) LPC dominates at deep levels, imbrication prevails at shallow levels.
3) Layers shortened above a weak, viscous substrate undergo less LPC relative to those shortened above a frictional dêcollement.
4) Penetrative strain varies in space (vertically and laterally), in time, with the type of modeling granular material, and with bulk shortening. At any given time, LPC is accommodated mainly within the youngest of the imbricate sheets.

In the sand layers of the models, LPC is accommodated by volume loss through porosity reduction. In nature, as documented from many thrust belts, this secondary (tectonic) compaction is likely to be accommodated by volume loss through pressure solution and porosity reduction, although a significant component of layer-parallel shortening may be balanced by layer thickening. This compactional deformation mechanism plays a significant role in determining the porosity and permeability of reservoir rocks in fold-thrust belts.

When applied to nature, our model results indicate that penetrative strain is heterogeneous in space and time in fold-thrust belts. Analyses of strain markers in the Spanish Pyrenees show that as much as 20% of the bulk shortening may be accommodated by LPS in the external areas.

ACKNOWLEDGMENTS

Thanks are due to Professors C.J. Talbot and Dr. A. Skelton for reading and commenting on this manuscript. This manuscript benefited from the critical and thorough reviews and useful suggestions of Peter Cobbold and Fabrizio Storti. The Université Paris-Sud financed a visit by HAK to Orsay. The Swedish Research Council (VR) has funded HAK.

REFERENCES CITED

Alonso, J. L., and A. Teixell, 1992, Forelimb deformation in natural examples of fault-propagation folds. , *in* K. R. McClay, ed., Thrust tectonics: London, Chapman & Hall, p. 175–180.

Baker, D. M., R. J. Lillie, S. R. Yeats, G. D. Johnson, M. Yousuf, and A. S. H. Zamin, 1988, Development of the Himalayan frontal thrust zone: Salt Range, Pakistan: Geology, v. 16, p. 3–7.

Bulat, J., and S. J. Stoker, 1987, Uplift determination from interval velocity studies, *in* J. Brooks and K. Glennie, eds., Petroleum geology of North West Europe, Graham and Trotman, London, p. 293–305.

Casas, J. M., D. Durney, J. Ferret, J., and J. A. Muñoz, 1996, Determinación de la deformación finita en la vertiente sur del Pirineo oriental a lo largo de la transversal del río Ter: Geogaceta, v. 20 (4), p. 803–805.

Cobbold, P., E. Rossello, and B. Vendeville, 1989, Some experiments on interacting sedimentation and deformation above salt horizons: Bulletin Societ Geologique France, v. V, p. 453–460.

Colletta, B., J. Letouzey, R. Pinedo, J. F. Ballard, and P. Balé, 1991, Computerized X-ray tomography analysis of sandbox models: Examples of thin-skinned thrust systems: Geology, v. 19, p. 1063–1067.

Cooper, M. A., 1983, The calculation of bulk strain in oblique and inclined balanced sections: Journal of Structural Geology, v. 5, p. 161–165.

Cooper, M. A., M. R. Garton, and J. R. Hossack, 1983, The origin of the Basse Normandie duplex, Boulonnais, France: Journal of Structural Geology, v. 5, p. 139–152.

Cotton, J., and H. A. Koyi, 2000, Modeling thrust fronts above ductile and frictional detachments: Application to structures in the Salt Range and Potwar Plateau, Pakistan: Geological Society of America Bulletin, v. 112, p. 351–363.

Coward, M. P. and J. H.,Kim, 1981, Strain within thrust sheets, *in* K. R. McClay and N. J. Price, eds., Thrust and nappe tectonics: an international conference: Geological Society of London Special Publication 9, p. 275–292.

Dahlen, F. A., J. Suppe, and D. M. Davis, 1984, Mechanics of fold and-thrust belts and accretionary wedges (continued): Cohesive Coulomb Theory: Journal of Geophysical Research, v. 89, p. 10087–10101.

Dahlstrom, C. D. A., 1969, Balanced cross sections: Canadian Journal of Earth Sciences, v. 6, p. 743–747.

Davis, D., J. Suppe, and F. A. Dahlen, 1983, Mechanics of fold-and-thrust belts and accretionary wedges: Journal of Geophysical Research, v. 88, p. 1153–1172.

Dixon, J., 1982, Regional structural synthesis, Wyoming salient of western overthrust belt: AAPG Bulletin, v. 66, p. 1560–1580.

Durney, D. W., 1995, GRFRFP: a program for statistical analysis and plotting of elliptical shape data, version 5.4, December 1995. Barcelona University, Barcelona, Spain (unpublished).

Elliott, D., 1976, The energy balance and deformation mechanisms of thrust sheets: Royal Society of London Philosophical Transactions, series A, v. 283, p. 289–312.

Ellis, P. G., and K. R. McClay, 1988, Listric extensional fault systems—results of analogue model experiments: Basin Research, v. 1, p. 55–70.

Evans, M. A., and W. M. Dunne, 1991, Strain factorization and partitioning in the North Mountain thrust sheet, central Appalachia, U.S.A.: Journal of Structural Geology, v. 13, p. 21–35.

Fischer, M. W., and M. P. Coward, 1982, Strains and folds within thrust sheets: an analysis of the Heilam sheet, northwest Scotland, *in* G. D. Williams, ed., Strain within thrust belts: Tectonophysics, v. 88, p. 291–312.

Gary, M. B., and G. Mitra, 1993, Migration of deformation fronts during progressive deformation: evidence from detailed structural studies in the Pennsylvania Anthracite region, U.S.A.: Journal of Structural Geology, v. 15, no. 3–5, p. 435–449.

Geiser, P. A., 1988a, Mechanisms of thrust propagation: some examples and implications for the analysis of overthrust terranes: Journal of Structural Geology, v. 10, p. 829–845.

Geiser, P. A., 1988b, The role of kinematics in the construction and analysis of geological cross sections in deformed terranes, *in* G. Mitra and S. Wojtal, eds., Geometries and mechanisms of thrusting: Geological Society of America Special Paper 222, p. 47–76.

Gutscher, M. A., N. Kukowiski, J. Malavieille, and S. Lallemand, 1996, Cyclical behaviour of thrust wedges: Insight from basal friction sandbox experiments: Geology, v. 24, p. 35–138.

Helmstedt, H., and R. G. Greggs, 1980, Stylolitic cleavage and cleavage refraction in lower Paleozoic carbonate rocks of the great valley, Maryland: Tectonophysics, v. 66, p. 99–114.

Homza, T. X., and W. K. Wallace, 1997, Detachment folds with fixed hinges and variable detachment depth, northeastern Brooks Range, Alaska: Journal of Structural Geology, v. 19, p. 337–354.

Horsfield, W. T., 1977, An experimental approach to basement controlled faulting: Geologie en Mijnbouw, v. 56, p. 363–370.

Hossack, J. R., 1978, The correction of stratigraphic sections for tectonic finite strain in the Bygdin area, Norway: Journal of the Geological Society of London, v. 135, p. 229–241.

Hossack, J. R., 1979, The use of balanced cross section in the calculation of orogenic contraction: Journal of Geological Society of London, v. 136, p. 705–711.

Howard, J. H., 1993, Restoration of cross sections through unfaulted, variably strained strata: Journal of Structural Geology, v. 15, p. 1331–1342.

Hubbert, K., 1937, Theory of scaled models as applied to geologic structures: Geological Society of America Bulletin, v. 48, p. 1459–1519.

Hubbert, K., 1951, Mechanical basis for certain familiar geological structures: Geological Society of America Bulletin, v. 62, p. 355–372.

Jaswal, T. J., R. J. Lillie, and R. D. Lawrence, 1997, Structure and evolution of the northern Potwar deformed zone, Pakistan: AAPG Bulletin, v. 81, p. 308–328.

Karig, D. E., 1986, Physical properties and mechanical state of accreted sediments in the Nankai Trough, Southwest Japan Arc: Geological Society of America Memoir 166, p. 117–133.

Karig, D.E., and N. Lundberg, 1990, Deformation bands from the toe of the Nankai accretionary prism: Journal of Geophysical Research, v. 95 (B6), p. 9099–9109.

Kilsdonk, B., and D. V. Wiltschko, 1988, Deformation mechanisms in the southeastern ramp region of the Pine Mountain Block, Tennessee: Geological Society of America Bulletin, v. 100, p. 653–664.

Koyi, H., 1995, Mode of internal deformation in sand wedges: Journal of Structural Geology, v. 17, p. 293–300.

Koyi, H. A., 2000, Towards dynamic restoration of geologic profiles: some lessons from analogue modeling, *in* M. Webster and M. Talwani, eds., Atlantic Rifting and Continental Margins, Geophysical Monograph Series, v. 115, p. 334.

Koyi, H. A., K. Hessami, and A. Teixell, 2000, Epicenter distribution and magnitude of earthquakes in fold-thrust belts: insights from sandbox model, Geophysical Research letters, v. 27, p. 273–276.

Liu, H., K. R. McClay, and D. Powell, 1991, Physical models of thrust wedges, *in* K. R. McClay, ed., Thrust tectonics: London, Chapman & Hall, p. 71–81.

Lohrmann, J., N. Kukowski, J. Adam, and O. Onken, 2003, The impact of analogue material properties on the geometry, kinematics, and dynamics of convergent sand wedges: Journal of Structural Geology, v. 25, p. 1691–1711.

Malavieille, J., 1984, Modélisation experimentale des chevauchements imbriqués: Application aux chaines de montagnes: Geological Society of France Bulletin, v. 7, p. 129–138.

Mandl, G., 1988, Mechanics of tectonic faulting: Elsevier, Amsterdam, 407 p.

Marshak, S., and T. Engelder, 1985, Development of cleavage in a fold-thrust belt in eastern New York: Journal of Structural Geology, v. 7, p. 345–359.

Marshak, S., and N. B. Woodward, 1988, Introduction to cross section balancing, in basic methods, *in* S. Marshak and G. Mitra, eds., Structural geology: Engelwood Cliffs, NJ, Prentice Hall, p. 303–332.

McClay, K. R., 1990, Deformation mechanics in analogue modelsof extensional fault systems, *in* R. J. Knipe and E. H. Rutter, eds., Deformation mechanisms, rheology and tectonics: Geological Society of London Special Publication 54, p. 445–453.

McClay, K. R., and P. G. Ellis, 1987, Geometries of extensional fault systems developed in model experiments: Geology, v. 15, p. 341–344.

McNaught, M. A., and G. Mitra, 1996, The use of finite strain data in constructing a retrodeformable cross-section of the Meade thrust sheet, southeastern Idaho, U.S.A.: Journal of Structural Geology, v. (18)5, pp. 573–583.

Meigs, A., J. Verges, and D. W. Burbank, 1996, Ten-million-year history of a thrust sheet: Geological Society of America Bulletin, v. 108, p. 1608–1625.

Menpes, R. J., and R. R. Hillis, 1995, Qualification of Tertiary exhumation from sonic velocity data, Celtic Sea/south-Western Approaches, *in* J. G. Buchanan and P. G. Buchanan, eds., Basin inversion: Geological Society of London Special Publication 88, p. 191–207.

Miralles, L., 1999, Estudi de la fàbrica de roques d' halita: aplicació a la conca Potàssica Catalana: Unpublished Ph.D. Thesis, Universitat de Barcelona, 213 p.

Mitra, G., 1978a, Ductile deformation zones and mylonites: the mechanical processes involved in the deformation of crystalline basement rocks: American Journal of Science, v. 278, p 1057–1084.

Mitra, S., 1978b, Microscopic deformation mechanisms and flow laws in quartzites within the South Mountain anticline: Journal of Geology, v. 86, p. 129–152.

Mitra, S., 1988, Effects of deformation mechanisms on reservoir potential in central Appalachian overthrust belt: AAPG Bulletin, v. 72, p. 536–554.

Mitra, S., 1990, Fault propagation folds: Geometry, kinematic evolution and hydrocarbon traps: AAPG Bulletin, v. 74, p. 921–945.

Mitra, G., 1994, Strain variation in thrust sheets across the Sevier fold-and-thrust belt (Idaho-Utah-Wyoming): implications for section restoration and wedge taper evolution: Journal of Structural Geology, v. 6, p. 51–61.

Mitra, G., and D. Elliott, 1980, Deformation of basement in the Blue Ridge and the development of the South Mountain cleavage, *in* D. R. Wones, ed., Proceedings of ''TheCaledonides in the USA'' Memoir, v. 2: Virginia Polytechnic Institute, Department of Geological Sciences, p. 307–311.

Mitra, G., W. A. Yonkee, and D. J. Gentry, 1984, Solution cleavage and its relationship to major structures in the Idaho-Wyoming-Utah thrust belt: Geology, v. 12, p. 354–358.

Moretti, I., S. Wu, and A. W. Bally, 1990, Computerised balanced cross section LOCACE to reconstruct an allochthonous salt sheet, offshore Louisiana: Marine and Petroleum Geology, p. 371–377.

Morley, C. K., 1986, A classification of thrust fronts: AAPG Bulletin, v. 70, p. 12–25.

Mukul, M., and G. Mitra, 1998, Finite strain and strain variation analysis in the Sheeprock thrust sheet; an internal thrust sheet in the Provo salient of the Sevier fold-and-thrust belt, central Utah: Journal of Structural Geology, v. 20, p. 385–405.

Mulugeta, G., 1988, Modeling the geometry of Coulomb thrust wedges: Journal of Structural Geology, v. 10, p. 847–859.

Mulugeta, G., and H. Koyi, 1987, Three-dimensional

geometry and kinematics of experimental piggyback thrusting: Geology, v. 15, p. 1052–1056.
Mulugeta, G., and H. Koyi, 1992, Episodic accretion and strain partitioning in a model sand wedge: Tectonophysics, v. 202, p. 319–333.
Nickelsen, R. P., 1986, Cleavage duplexes in the Marcellus shale of the Appalachian foreland: Journal of Structural Geology, v. 8, p. 361–371.
Price, R. A., 1981, The Cordilleran foreland thrust and fold belt in the southern Canadian Rocky Mountains, *in* K. McClay and R. A. Price, eds., Thrust and nappe tectonics: Geological Society of London Special Publication 9, p. 427–448.
Protzman, G. M., and G. Mitra, 1990, Strain fabric associated with the Meade thrust sheet: implications for cross-section balancing: Journal of Structural Geology, v. 12, p. 403–417.
Ramsay, J. G., and M. I. Huber, 1987, The techniques of modern structural geology, volume 2, Folds and fractures: Oxford, Academic Press, 700 p.
Sanderson, D. J., 1982, Models of strain variation in nappes and thrust sheets: A review: Tectonophysics, v. 88, p. 201–233.
Sáez, A., 1987, Estratigrafía y sedimentología de las formaciones lacustres del tránsito Eoceno Oligoceno del NE de la Cuenca del Ebro. PhD thesis. Universitat de Barcelona, 352 p.
Sans, M., 1999, From thrust tectonics to diapirism. The role of evaporites in the kinematic evolution of the Eastern South-Pyrenean front: Unpublished PhD Thesis Universitat de Barcelona, 197 p.
Sans, M., and J. Vergés, 1995, Fold development related to contractional salt tectonics southeastern Pyrenean thrust front, Spain, in M. P. A. Jackson, D. G. Roberts, and S. Snelson, eds., Salt tectonics: a global perspective: AAPG memoir 65, p. 369–378.
Sans, M., J. A. Muñoz, and J. Verges, 1996, Triangle zone and thrust wedge geometries related to evaporitic horizons (southern Pyrenees): Bulletin of Canadian Petroleum Geology, v. 44 (2), p. 375–384.
Storti, F., and K. McClay, 1995, The influence of sedimentation on the growth of thrust wedges in analogue models: Geology, v. 23, p. 999–1002.
Storti, F., F. Salvini, and K. McClay, 1997, Fault related folds in sandbox analogue models of thrust wedges: Journal of Structural Geology, v. 19, p. 583–602.
Suppe, J., 1983, Geometry and kinematics of fault-bend folding: American Journal of Science, v. 283, p. 684–721.
Suppe, J., 1985, Principles of structural geology: Englewood Cliffs, New Jersey, Prentice Hall, 537 pp.
Teixell, A., 1996, The Ansó transect of the southern Pyrenees: basement and cover thrust geometries: Journal of Geological Society of London, v. 153, p. 301–310.
Teixell, A., and H. A. Koyi, 2003, Experimental and Field study of the effects of lithological contrasts on thrust-related deformation: Tectonics, v. 22, p. 1054–1073.
Thorbjornsen, K. L., and W. M. Dunne, 1997, Origin of a thrust-related fold: geometric vs, kinematic tests: Journal of Structural Geology, v. 19, p. 303–319.
Tonghban, H., 2000, Estude du soulevement au neogene de la bordure continentale norvegienne: approche stratigraphique et quantification, Ph.D. thesis, Université Paris-Sud, 320 p.
Turcotte, D. L. and G. Schubert, 1982, Geodynamics: New York, J. Wiley & Sons, 450 p.
Vergés, J. 1993, Estudi geologic del vessant sud del Pirineu oriental i central. Evolució cinemàtica en 3·D. Unpublised Ph.D. thesis, Universitat de Barcelona, 203 p.
Vergés, J., M. Marzo, T. Santaeulària, J. Serra-Kiel, D. W. Burbank, J. A. Muñoz, and J. Giménez-Montsant, 1998, Quantified vertical motions and tectonic evolution of the SE Pyrenean foreland basin., *in* A. Mascle, C. Puigdefàbregas, H. P. Luterbacher, and M. Fernàndez, eds., Cenozoic foreland basins of Western Europe: Geological Society of London Special Publication 134, p. 107–134.
Weijermars, R., 1986, Flow behavior and physical chemistry of bouncing putties and related polymers in view of tectonic laboratory applications: Tectonophysics, v. 124, p. 325–358.
Weijermars, R., M. P. A. Jackson, and B. Vendeville, 1993, Rheological and tectonic modeling of salt provinces: Tectonophysics, v. 217, p. 143–174.
Williams, G. D., and T. J. Chapman, 1983, Strain developed in the hanging walls of thrusts due to slip/propagation rate: a dislocation model: Journal of Structural Geology, v. 5, p. 563–571.
Wiltschko, D. V., 1981, Thrust sheet deformation at a ramp: summary and extension of an earlier model, *in* K. R. McClay and N. J. Price, eds., Thrust and nappe tectonics, Geological Society of London Special Publication 9, p. 55–64.
Wissinger, E. S., A. R. Levander, J. S. Oldow, G. S. Fuis, and W. J. Lutter, 1998, Seismic profiling constraints on the evolution of central Brooks Range, Arctic Alaska, *in* J. S. Oldow and H. G. Lallemant, eds., Architecture of the Central Brooks Range fold and thrust belt, Arctic Alaska, Geological Society of America Special Paper, 324, p. 269–291.
Woodward, N. B., S. E. Boyer, and J. Suppe, 1985, An outline of balanced cross sections, 2nd edition: University of Tennessee Department of Geological Sciences Studies in Geology, 11, 170 p.
Woodward, N. B., D. R. Grey, and D. B. Spears, 1986, Including strain data in balanced cross-sections: Journal of Structural Geology, v. 8, p. 313–324.
Woodward, N. B., S. E. Boyer, and J. Suppe, 1989, Structural lithic units in external orogenic zones: Tectonophysics, v. 158, p. 247–267.
Zhao, W. L., D. M. Davis, F. A. Dahlen, and J. Suppe, 1986, Origin of convex accretionary wedges: evidence from Barbados: Journal of Geophysical Research, v. 91, p. 10246–10258.